Fast experimental identification of suspension models for control design

C Crivellaro[1] and **D C Donha**[2]*
[1]Technology of Commercial Vehicles, Product Development/Technology, Metalsa Brazil, Osasco, Brazil
[2]Dynamic and Control Laboratory, Department of Mechanical Engineering, Escola Politecnica, University of São Paulo, São Paulo, Brazil

The manuscript was received on 12 January 2010 and was accepted after revision for publication on 14 October 2010.

DOI: 10.1177/2041299110393176

Abstract: This paper presents both the theoretical and the experimental approaches of the development of a mathematical model to be used in multi-variable control system designs of an active suspension for a sport utility vehicle (SUV), in this case a light pickup truck. A complete seven-degree-of-freedom model is successfully quickly identified, with very satisfactory results in simulations and in real experiments conducted with the pickup truth. The novelty of the proposed methodology is the use of commercial software in the early stages of the identification to speed up the process and to minimize the need for a large number of costly experiments. The paper also presents major contributions to the identification of uncertainties in vehicle suspension models and in the development of identification methods using the sequential quadratic programming, where an innovation regarding the calculation of the objective function is proposed and implemented.

Results from simulations of and practical experiments with the real SUV are presented, analysed, and compared, showing the potential of the method.

Keywords: suspension models, control design, sport utility vehicle, expermental identification of models

1 INTRODUCTION

In this paper, a mathematical model with seven degrees of freedom (DOFs) for a sport utility vehicle (SUV) is identified using experimental data, such as vehicle body accelerations and relative displacements of suspension elements. The model is intended to be used in the development of control system algorithms, e.g. in active suspension systems.

In recent years, several studies on the modelling and simulation of active and semi-active suspension systems have been published. Most of these use the traditional quarter-car model with two DOFs and different kinds of control approach [**1**, **2**]. Other investigations, probably rather concerned with a broader simulation of vehicle than with controls, use half-car models with four DOFs to include, for example, motions such as roll or pitch [**3**–**7**]. Also many studies use a four-wheel model for the vehicle controller development, but do not use a multiple-input multiple-output (MIMO) control strategy, although some of these deal with over-actuated systems, when an optimal distribution of forces among actuators would be interesting and relevant [**8**, **9**].

In general, it is mandatory in the design of a control system to obtain low-order dynamic models, mainly to reduce the computer burden and to enhance the controller performance. This is also the case for active suspension control systems, which usually require very fast processing algorithms. The aim is thus to reach the simplest model that is able to reproduce with reasonable accuracy the behaviour of the real vehicle, including the important effect of

*Corresponding author: Dynamic Control Laboratory, Department of Mechanical Engineering, University of São Paulo, Escola Politecnica, São Paulo 05508-970, Brazil.
email: decdonha@usp.br

coupling between the motions and the interaction between variables.

Many control algorithms are based on a linear time-invariant model of the vehicle. Control strategies, such as H_∞, hybrid H_2-H_∞, linear quadratic gaussian (LQG)–loop transfer recovery (LTR), or even classical control approaches, to list the most important, need a mathematical model that it as simple as possible but is able to reproduce with sufficient accuracy the real system to be controlled. In robust controller synthesis, the search for a suitable model and its uncertainties accounts for almost 60 per cent of the control design work. In the control of automotive suspensions, the use of models with a large number of DOFs is very common, but it is not trivial to guarantee the desirable matching of results of the theoretical model and the behaviour of the real vehicle. Therefore, an important advantage of the robust approaches is to take the uncertainties into account already in the synthesis stage.

Generally, any control system involving uncertainties can be put in the form shown in Fig. 1, which is the basis for the controller design.

The input vector $\boldsymbol{u}_1$ in Fig. 1 represents the exogenous signals acting upon the system; $\boldsymbol{u}_2$ is the control input vector. The set of outputs $\boldsymbol{y}_1$ is known as the performance output vector to be controlled and $\boldsymbol{y}_2$ is the vector of the measurable outputs. The output $\boldsymbol{y}_3$ and input $\boldsymbol{u}_3$ are signals of the feedback loop which represent the uncertainty dynamics.

In Fig. 1, the block in the middle represents the nominal plant to be controlled by the lower block, i.e. the controller. No physical system can be exactly represented by a mathematical model. The degree to which a nominal model represents the physical system is qualified by an uncertainty bound. In Fig. 1, the upper block is included to describe the model uncertainties.

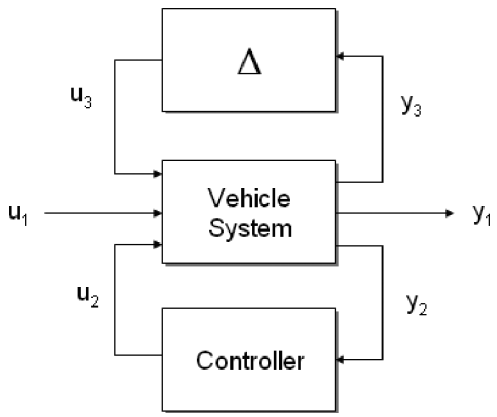

Fig. 1 Two-port configuration

System identification for the purpose of robust control design involves the estimation of a nominal model for the real system and also the uncertainty bounds of that nominal model via the use of experimentally measured input–output data. Although many algorithms have been developed to identify nominal models, little effort has been directed towards identifying uncertainty bounds. A major contribution of this work is the development of methodologies for both nominal and multi-variable uncertainty model identification.

Another important contribution of this work is the idea to use full-vehicle simulation software to identify a low-control model, avoiding the need for real vehicle tests in a ground field in the early stages of the project, with a clear reduction in the cost design. Many complex and very complete vehicle models are available as commercial software. It is important to point out that at this stage any good software, such as CALLAS/PROSPER, CARSIM, or any other similar package used, for example, in homologation tests, would perform adequately. The objective here is only to obtain a preliminary set of qualified data, which is used to feed the proposed identification algorithm. Since the model created by commercial simulator software produces data with good correlation with experimental data, it is possible to use the models with confidence to obtain valuable information about a real vehicle, avoiding extra costs with acquisition of new experimental data and saving time in a preliminary development phase. In this work, couplé à la limite d'adhésion au sol (CALLAS, software from the French corporation Société d'Études et Réalisations Automobiles (SERA-CD)), a simulation package used in the studies of the dynamics of cars, trucks, and army vehicles, was utilized.

Another contribution, which is perhaps more important, is the development of a practical technique of model identification, based on sequential quadratic programming (SQP) [**10**]. The approach used here brings an innovation regarding the calculation of the objective function and the goal attainment method (GAM) that can be posed as a non-linear programming problem inspired by reference [**11**]. The SQP algorithm aims basically to minimize the 'cost' of the quadratic error between signals produced by commercial software (or real data at a more advanced stage) and signals produced by a simplified model, working under the same disturbances.

After the validation of the model through numerical simulation procedures and evidence that the proposed methodology is reliable and produces data with good correlation regarding the vehicle,

a few ground tests are conducted for online identification using the real vehicle and for final validation of the methodology. It is then possible to use the identified model with confidence in further developments, e.g. in control designs.

Using the proposed methodology, a low-order vehicle model for an SUV with a seven-DOF model was identified through the determination of 13 parameters, basically the masses and moments of inertia, the spring stiffnesses, and the damping coefficients related to the vehicle suspension. This may be seen as a simple task, considering that many of these parameters can be easily calculated or measured. However, the practice of defining lumped parameters equal to the individual component values is often an unhelpful approach, since it does not take into consideration the suspension configuration and the interaction and coupling of parts in the whole vehicle. For example, it is easy to measure the wheel mass, but it is quite difficult to know how much mass from the components of the suspension should be part of the unsprung mass or of the sprung mass.

Another advantage of the methodology is that simulation results are practical to tune models, since they can be generated free of noise, which is not the case within experimental data, for which, on the contrary, it is often necessary to filter noisy signals, with all the well-known problems involved.

As will be shown, the low-order model identified using the proposed methodology can effectively portray the behaviour of a real vehicle and is an adequate basis for a centralized MIMO control synthesis.

2 SUV MATHEMATICAL MODEL

In this section, the development of a mathematical model to be used in a centralized model controlled system of an active or semi-active SUV suspension is presented. This model is called the low-order model, in contrast with higher-order models available as commercial software.

The development of a complete vehicle model for suspension control design has to consider the following assumptions.

1. The model represents the whole vehicle, including its four wheels.
2. The input of exogenous disturbances is modelled as signal of vertical velocities, according to the Thompson [**12**] model.
3. The control inputs are modelled as forces applied between the wheels (unsprung masses) and the vehicle body (sprung mass), only in the damper position.
4. The model considers the front anti-roll bar and the rear axle; this greatly affects the vehicle behaviour and cannot be disregarded.
5. The model provides as measured outputs the vertical accelerations at four points in the vehicle body over each wheel (for comfort evaluation), the relative displacement between each wheel and the vehicle body (for 'stroke' amplitude evaluation), and the vertical acceleration of wheels.
6. The model provides as non-measured outputs four relative displacements between the centre of each wheel and its contact point with the road (for adherence evaluation).

To comply with the previous assumptions, the physical model shown in Fig. 2 was used. The sprung body is modelled by a rigid body, sustained by four unsprung masses associated with the wheels. Suspension elements are considered to be linear and pure. The parameters in Fig. 2 are presented in Table 1.

For simplicity, it is assumed that the vehicle sprung body has only three DOFs, namely heave, roll, and pitch, and that the wheels can perform only vertical movements, which then leads to a seven-DOF model. In Fig. 2, $\boldsymbol{z}_{01}(t)$ is a vector with four relative displacements between the ground and each wheel and is a $\boldsymbol{z}_{12}(t)$ vector with relative displacements between the centre of each wheel and the point of connection of the respective wheel suspension in the vehicle body. Likewise, $\dot{\boldsymbol{z}}_{01}(t)$ and $\dot{\boldsymbol{z}}_{12}(t)$ define the relative velocities; also $\dot{\boldsymbol{z}}_0(t)$ is the vector of vertical velocities applied by the ground in each wheel and $\dot{\boldsymbol{z}}_1(t)$ is the vector composed of the vertical velocities of the front wheels, the vertical velocity of the rear axis, and its angular velocity. The vector $\boldsymbol{\xi}(t)$ is given by $\boldsymbol{\xi}(t)=[z_{\mathrm{CG}}(t) \quad \varphi(t) \quad \theta(t)]^{\mathrm{T}}$, where $z_{\mathrm{CG}}(t)$ is the heave motion of the centre of gravity, $\varphi(t)$ is the pitch, and $\theta(t)$ is the roll angle of the vehicle body (sprung mass).

To facilitate reading, the motion variables $z_{\mathrm{CG}}(t), \phi(t),$ *and* $\theta(t)$ of the sprung body are shown in Fig. 3.

The low-order vehicle model can be briefly expressed by the equations

$$\mathbf{M}_1\ddot{\boldsymbol{z}}_1(t)=\mathbf{L}_1^{\mathrm{T}}\boldsymbol{F}_1(t) \tag{1}$$

$$\mathbf{M}_2\ddot{\boldsymbol{\xi}}(t)=\mathbf{L}_2^{\mathrm{T}}\boldsymbol{F}_2(t) \tag{2}$$

where $\mathbf{M}_1=\mathrm{diag}(m_1, m_1, m_3, J_3)$ is the diagonal inertia matrix containing the two front wheel masses, the rear axle mass, and its moment of inertia respectively, $\mathbf{M}_2 = \mathrm{diag}(m_2, J_\phi, J_\theta)$ is the diagonal

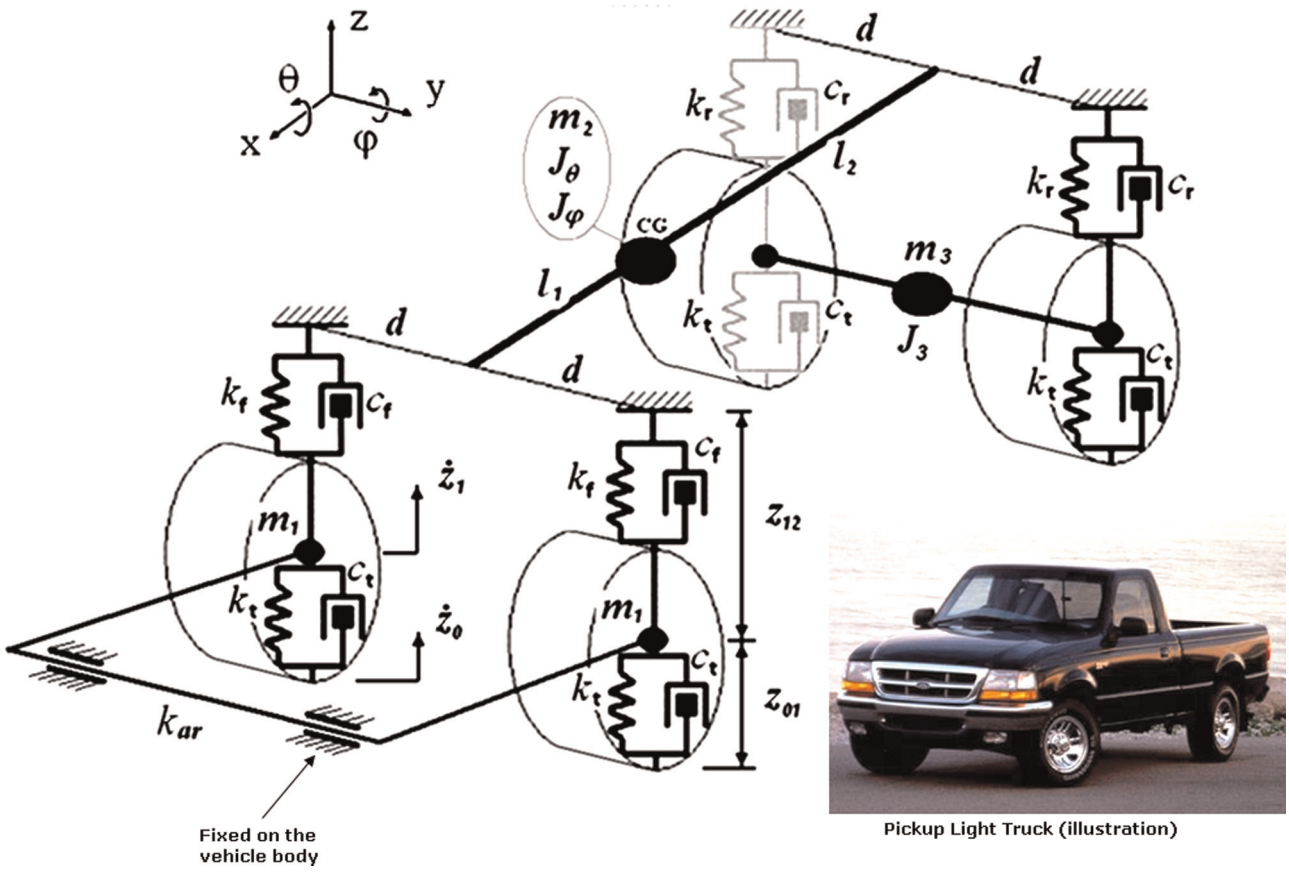

Fig. 2 Physical vehicle model with seven DOFs

Table 1 Parameters of the vehicle model

Parameter	Description	Unit
m_1	Front unsprung mass (wheels)	kg
m_2	Sprung mass	kg
m_3	Rear unsprung mass (axle and wheels)	kg
J_3	Rear unsprung inertia moment (x axis)	kg m^2
J_θ	Roll moment of inertia, sprung mass	kg m^2
J_φ	Pitch moment of inertia, sprung mass	kg m^2
k_t	Tyre stiffness coefficient	N/m
k_f	Front spring stiffness coefficient	N/m
k_r	Rear spring stiffness coefficient	N/m
k_{ar}	Anti-roll bar stiffness coefficient	N/m
c_t	Tyre damping coefficient	N s/m
c_f	Front damper damping coefficient	N s/m
c_r	Rear damper damping coefficient	N s/m
l_1	Front-axle distance from the centre of gravity	m
l_2	Rear-axle distance from the centre of gravity	m
d	Distance between the centre of gravity CG and the vehicle side	m
d_{se}	Rear semi-axle length	m

inertia matrix of the sprung mass (vehicle body), where m_2 is the sprung mass of the vehicle, J_φ is the moment of inertia of the sprung mass around the transverse vehicle y axis, J_θ is the moment of inertia of the sprung mass around the longitudinal vehicle x axis, $\boldsymbol{F}_1(t)$ is the vector of resultant forces in the wheels; $\boldsymbol{F}_2(t)$ are forces applied by the suspension in the vehicle sprung body; $\mathbf{L}_1$ is a transformation matrix relating $\dot{\boldsymbol{z}}_1(t)$ to the vertical velocities of the four wheels, and $\mathbf{L}_2$ is a transformation matrix relating the vertical displacements of the sprung vehicle body at the suspension connection points to heave, pitch, and roll displacements of the sprung mass $\mathbf{L}_1$ and $\mathbf{L}_2$ are given by

$$\mathbf{L}_1=\begin{bmatrix}1&0&0&0\\0&1&0&0\\0&0&1&d_r\\0&0&1&-d_r\end{bmatrix},\quad \mathbf{L}_2=\begin{bmatrix}1&-l_1&d\\1&-l_1&-d\\1&l_2&d\\1&l_2&-d\end{bmatrix} \tag{3}$$

where d_r is the length of the rear semi-axle, and l_1, l_2 and d are dimensions of the sprung body shown in Fig. 2. $\boldsymbol{F}_1(t)$ is given by

$$\boldsymbol{F}_1(t)=\mathbf{K}_{01}\boldsymbol{z}_{01}(t)-\mathbf{C}_{01}\mathbf{L}_1\dot{\boldsymbol{z}}_1(t)+\mathbf{C}_{01}\dot{\mathbf{z}}_0(t)-\boldsymbol{F}_2(t) \tag{4}$$

where $\mathbf{K}_{01}=\mathrm{diag}(k_t,k_t,k_t,k_t)$ is the diagonal matrix of the tyre stiffnesses, $\mathbf{C}_{01}=\mathrm{diag}(c_t,c_t,c_t,c_t)$ is the

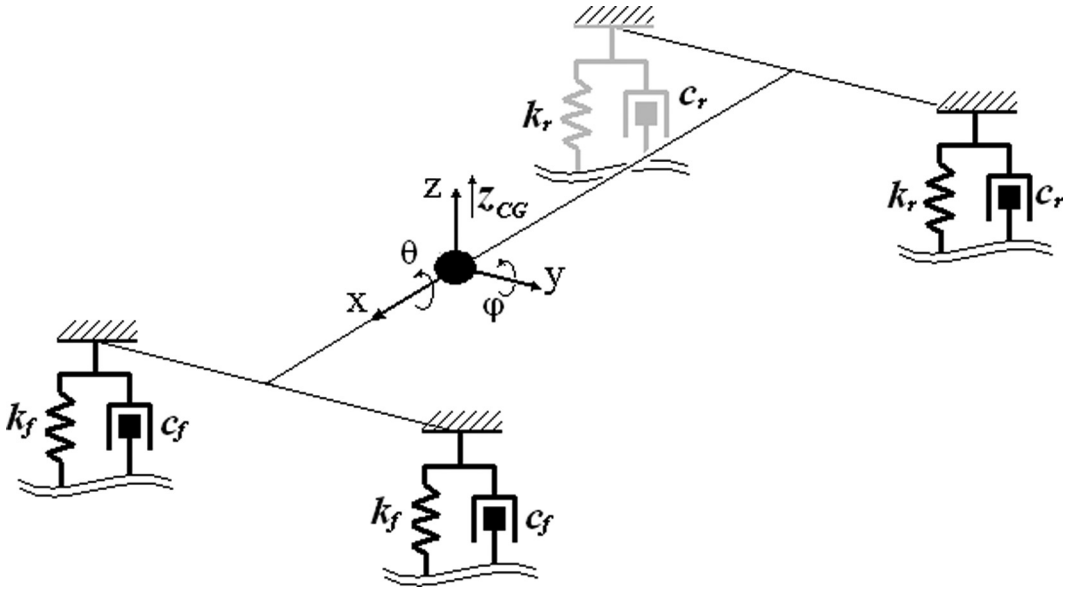

Fig. 3 Vehicle body motions

diagonal matrix of the damping coefficients of the tyres. $\boldsymbol{F}_2(t)$, the forces that the suspension applies in the vehicle sprung body, is given by

$$\boldsymbol{F}_2(t)=\mathbf{K}_{12}\boldsymbol{z}_{12}(t)+\mathbf{C}_{12}\dot{\boldsymbol{z}}_{12}(t) \tag{5}$$

where $\mathbf{C}_{12}=\mathrm{diag}(c_\mathrm{f}, c_\mathrm{f}, c_\mathrm{f}, c_\mathrm{f})$ is the diagonal matrix of damping coefficients of the dampers, where the subscript f indicates font, the subscript r indicates rear, and $\mathbf{K}_{12}$ is the diagonal matrix of the spring stiffnesses given by

$$\mathbf{K}_{12}=\begin{bmatrix} k_\mathrm{f}+k_\mathrm{tb} & -k_\mathrm{tb} & 0 & 0 \\ -k_\mathrm{tb} & k_\mathrm{f}+k_\mathrm{tb} & 0 & 0 \\ 0 & 0 & k_\mathrm{r} & 0 \\ 0 & 0 & 0 & k_\mathrm{r} \end{bmatrix}$$

where k_tb is the stiffness coefficient of the torsion bar, an anti-roll device.

Defining the disturbance inputs in the wheels as $\boldsymbol{w}(t) \triangleq \dot{\boldsymbol{z}}_0(t)$ and the state vector as

$$\boldsymbol{x}(t)=\begin{bmatrix}\boldsymbol{z}_{01}(t) & \boldsymbol{z}_{12}(t) & \dot{\boldsymbol{z}}_1(t) & \dot{\boldsymbol{\xi}}(t)\end{bmatrix}^\mathrm{T} \tag{6}$$

equations (4) and (5) can be rewritten as

$$\boldsymbol{F}_1(t)=\mathbf{R}_1\boldsymbol{x}(t)+\mathbf{C}_{01}\boldsymbol{w}(t) \tag{7}$$

$$\boldsymbol{F}_2(t)=\mathbf{R}_2\boldsymbol{x}(t) \tag{8}$$

where

$$\mathbf{R}_1=\begin{bmatrix}\mathbf{K}_{01} & -\mathbf{K}_{12} & -(\mathbf{C}_{01}-\mathbf{C}_{12})\mathbf{L}_1 & \mathbf{C}_{12}\mathbf{L}_2\end{bmatrix} \tag{9}$$

$$\mathbf{R}_2=\begin{bmatrix}\mathbf{0}_{4x4} & \mathbf{K}_{12} & \mathbf{C}_{12}\mathbf{L}_1 & -\mathbf{C}_{12}\mathbf{L}_2\end{bmatrix} \tag{10}$$

Equations (1) and (2) can be represented in the standard space state form, e.g. for future control system synthesis, as

$$\begin{aligned}\dot{\boldsymbol{x}}(t)&=\mathbf{A}\boldsymbol{x}(t)+\mathbf{B}_1\boldsymbol{w}(t)+\mathbf{B}_2\boldsymbol{u}(t)\\ \boldsymbol{y}_1(t)&=\mathbf{C}_1\boldsymbol{x}(t)+\mathbf{D}_{11}\boldsymbol{w}(t)+\mathbf{D}_{12}\boldsymbol{u}(t)\\ \boldsymbol{y}_2(t)&=\mathbf{C}_2\boldsymbol{x}(t)+\mathbf{D}_{21}\boldsymbol{w}(t)+\mathbf{D}_{22}\boldsymbol{u}(t)\\ \boldsymbol{y}_3(t)&=\mathbf{C}_3\boldsymbol{x}(t)+\mathbf{D}_{31}\boldsymbol{w}(t)+\mathbf{D}_{32}\boldsymbol{u}(t)\end{aligned} \tag{11}$$

where

$$\mathbf{A}=\begin{bmatrix}\mathbf{0}_{4\times4} & \mathbf{0}_{4\times4} & -\mathbf{L}_1 & \mathbf{0}_{4\times3} \\ \mathbf{0}_{4\times4} & \mathbf{0}_{4\times4} & \mathbf{L}_1 & \mathbf{L}_2 \\ & & \mathbf{M}_1^{-1}\mathbf{L}_1^\mathrm{T}\mathbf{R}_1 & \\ & & \mathbf{M}_2^{-1}\mathbf{L}_2^\mathrm{T}\mathbf{R}_2 & \end{bmatrix}$$

$$\mathbf{B}_1=\begin{bmatrix}\mathbf{I}_{4\times4} \\ \mathbf{0}_{4\times4} \\ \mathbf{M}_1^{-1}\mathbf{L}_1^\mathrm{T}\mathbf{C}_{01} \\ \mathbf{0}_{3\times4}\end{bmatrix}$$

$$\mathbf{B}_2=\begin{bmatrix}\mathbf{0}_{4\times4} \\ \mathbf{0}_{4\times4} \\ \mathbf{M}_1^{-1}\mathbf{L}_1^\mathrm{T} \\ \mathbf{M}_2^{-1}\mathbf{L}_2^\mathrm{T}\end{bmatrix} \tag{12}$$

$$\mathbf{C}_1=\begin{bmatrix}\mathbf{I}_{4\times4} & \mathbf{0}_{4\times11}\end{bmatrix}\quad \mathbf{C}_2=\begin{bmatrix}\mathbf{L}_2\mathbf{M}_2^{-1}\mathbf{L}_2^T\mathbf{R}_2\end{bmatrix}$$
$$\mathbf{C}_3=\begin{bmatrix}\mathbf{0}_{4\times4} & \mathbf{I}_{4\times4} & \mathbf{0}_{4\times7}\end{bmatrix} \tag{13}$$

$$\begin{aligned}&\mathbf{D}_{11}=\mathbf{D}_{21}=\mathbf{D}_{31}=\mathbf{D}_{12}=\mathbf{D}_{32}=\mathbf{0}_{4x4}\\ &\mathbf{D}_{22}=\begin{bmatrix}\mathbf{L}_2\mathbf{M}_2^{-1}\mathbf{L}_2^T\end{bmatrix}\end{aligned} \tag{14}$$

In the matrices above, $\mathbf{0}_{\bullet\times\bullet}$ and $\mathbf{I}_{\bullet\times\bullet}$ stand for the null and the identity matrices respectively with the

indicated dimensions. The output $\boldsymbol{y}_1(t)$ gives $\boldsymbol{z}_{01}(t)$, $\boldsymbol{y}_2(t)$ gives the sprung mass acceleration over each wheel, and $\boldsymbol{y}_3(t)$ gives $\boldsymbol{z}_{12}(t)$ In fact, $\boldsymbol{y}_1(t)$ is not used in the control loop, since it is very hard to measure.

In this work, to reproduce real features, actuators are assumed to generate axial forces with a residual damping coefficient c_a. The actuator time response is 5 ms, and, in comparsion with the system dynamics, it is considered sufficiently small to disregard in the model. Actuator forces $\boldsymbol{u}_i$ are applied concomitantly in both the sprung and the unsprung masses, as action and reaction forces. As shown in Fig. 4, an active actuator replaces the shock absorber (damper) in the vehicle model, but a residual damper is also maintained in the model.

The matrix $\mathbf{C}_{12}$ in equation (5) is then replaced by $\mathbf{C}_{12} = \text{diag}[c_a,c_a,c_a,c_a]$ in active controlled systems. In general, the residual damping coefficient c_a is considered to be at least four times smaller than c_f and c_r [**13**].

Figure 5 is a pictorial representation of the mathematical model, including the forces $\boldsymbol{U}(s)$ of the actuators, exogenous inputs $\boldsymbol{W}(s)$ and the system outputs $\boldsymbol{Y}_1(s)$ and $\boldsymbol{Y}(s)$.

The matrices $\mathbf{A}$, $\mathbf{B}_1$, $\mathbf{B}_2$, and $\mathbf{C}_1$ were defined in equations (11) to (14) the matrices $\mathbf{C}$ and $\mathbf{D}$ appearing in the block diagram in Fig. 5 consolidate the set of sensor outputs and are given by

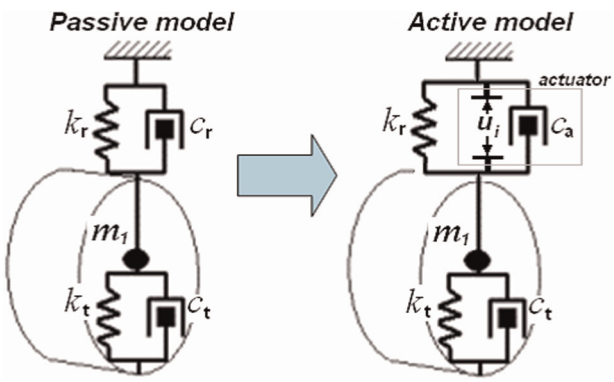

Fig. 4 Actuator model

$$\mathbf{C}=\begin{bmatrix}\mathbf{C}_2\\ \mathbf{C}_3\end{bmatrix}\quad \mathbf{D}=\begin{bmatrix}\mathbf{D}_{22}\\ \mathbf{D}_{32}\end{bmatrix}=\begin{bmatrix}\mathbf{D}_{22}\\ \mathbf{0}_{4\times 4}\end{bmatrix}$$

2.1 Exogenous signal models

A suitable description of the road disturbances is an important step in vehicular suspension modeling studies. The vehicle motions and attitudes are influenced by basically two kinds of disturbances: the road roughness and the various forces and momentum generated in abrupt manoeuvres, as cornering and braking, which change the vehicle direction or its velocity. At high velocities, the force generated by aerodynamic effects is also important.

Since the work is focused more on comfort than on manoeuvrability, only the road disturbances are considered in the vehicle modelling. The goal of comfort improvement can be considered as a filtering process of vibration effects generated by the road disturbances.

In the context of vibration, the road roughness is typically modelled by a stochastic signal with a determined power spectral density (PSD), which is added to the vertical displacement signal.

In the last 40 years, several models have been proposed to approximate PSD curves of road profiles, among which the models proposed in references [**14**] to [**16**] should be mentioned. However, for simplicity, the Thompson [**12**] model is used herein and is given by

$$S(\Omega)=A\Omega^n \tag{15}$$

where Ω is the spatial frequency (or the wave number), typically in units of radians per length, A is a parameter linked to the severity of road roughness, and n is a suitable constant.

According to the results obtained by Sevin and Pilkey [**17**], shown in Fig. 6, and Smith [**18**], shown in Fig. 7, the PSD curves of several kinds of by road can be represented approximately by a straight line, if a bilogarithm graph is used.

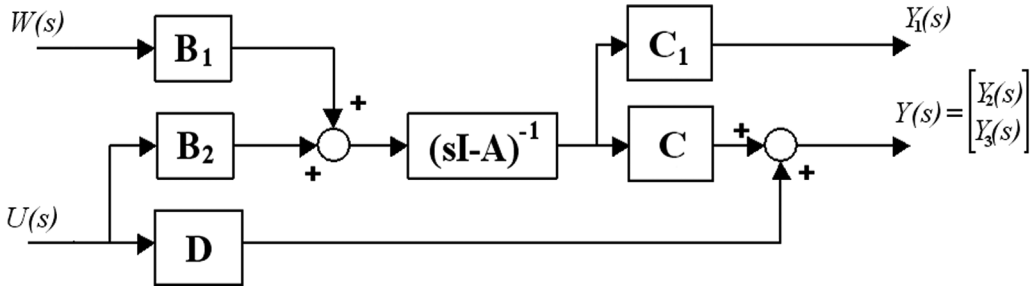

Fig. 5 Block diagram of the system model

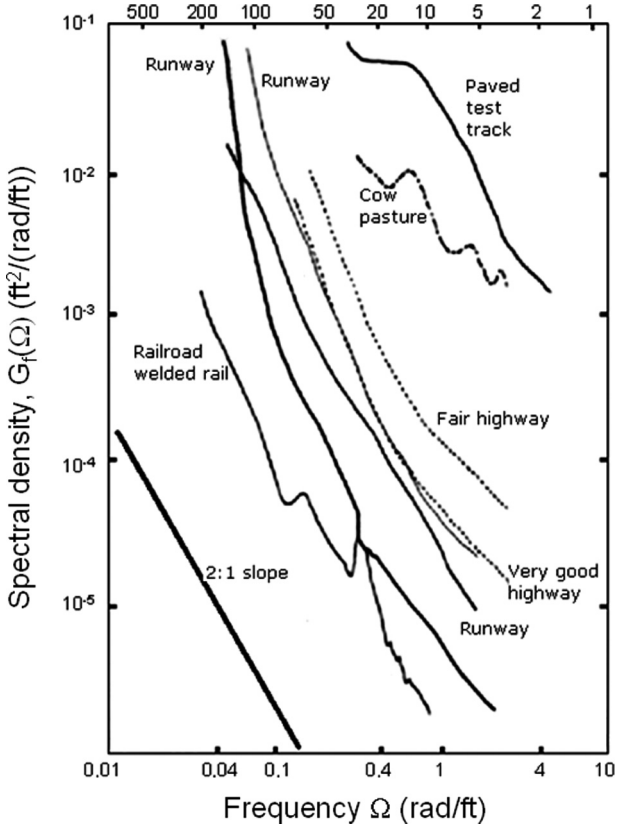

Fig. 6 PSD of various terrains (reproduced from Hrovat [**15**])

The negative inclination of these curves, representing the PSD of the vertical displacement signal, has a ratio of 2 to 1, which leads the parameter n in equation (15) to equal approximately -2; this implies that the vertical velocity signal should be represented by a white noise, since the vertical velocity is a time derivative of the vertical displacement signal. This is very convenient for some controller techniques such as the LQG, which consider the same hypothesis for the process noise. Thus, a more suitable mathematical model to represent the real vehicle should have vertical velocity signals as exogenous disturbances modelling the road roughness.

2.2 Leaf spring rear suspension

Rear suspensions based on a leaf spring, as shown in Fig. 8, are also called Hotchkiss suspensions. The Hotchkiss suspension is often used in pickup trucks, mainly because it is the cheapest and most robust type of rear suspension, but it does not have a good performance in comfort. This suspension has a significant part of its mass as unsprung mass, reducing the 'wheel hop' resonance frequency. In addition, the Coulomb friction between leaves is significant, which results in a hysteresis effect in the stiffness response curves of the springs [**19**]. Consequently, when a pickup truck runs on a good-quality road, the excitation may not be sufficient to overcome the static friction between the leaves, creating a higher value of the effective stiffness. This phenomenon increases the frequency of the sprung-mass vibration modes and reduces the comfort. The intrinsic non-linearity in this kind of rear suspension system creates severe difficulties in identifying a linear model.

3 MODEL IDENTIFICATION

In model identification problems, the use of modal parameter estimation algorithms is very common. One of the greatest difficulties in this problem is to determine the number of degrees of freedom of the system in the frequency range of interest, so that the modal parameter estimation algorithm can be accurately applied. In time-domain modal parameter estimation algorithms, such as the Ibrahim and Mikulcik [**20**] time domain, the polyreference time domain [**21**], and the eigensystem realization algorithm [**22**] methods, an overdetermined system equation is found to yield accurate results, without leading to a numerically unstable characteristic equation. In frequency-domain modal parameter estimation algorithms, such as the polyreference frequency domain [**23**] and the orthogonal polynomial [**24**–**27**], on the contrary, the characteristic equation does not present such nice features of numerical stability, and the attainment of accurate results depends on the correct selection of the system order.

An algorithm based on singular value decomposition applied to multiple-frequency response function measurements, known as the complex-mode identification function, was first developed for traditional multiple-frequency response function data to identify the proper order of the system equation [**27**, **28**]. Unlike the Multi-variate-mode indication function [**29**], which indicates the existence of real normal modes, complex-mode identification indicates the existence of real normal or complex normal modes and the relative magnitude of each mode.

Despite the efficiency of complex-mode identification, this method presents some inaccuracy when applied to systems with rigid bodies and non-linearities in the springs and dampers.

In the modal parameter estimation area, the modal parameters do not have any relationship to the physical parameters of the model. In a certain way, the lack of correlation between the identified parameter and the physical parameter is

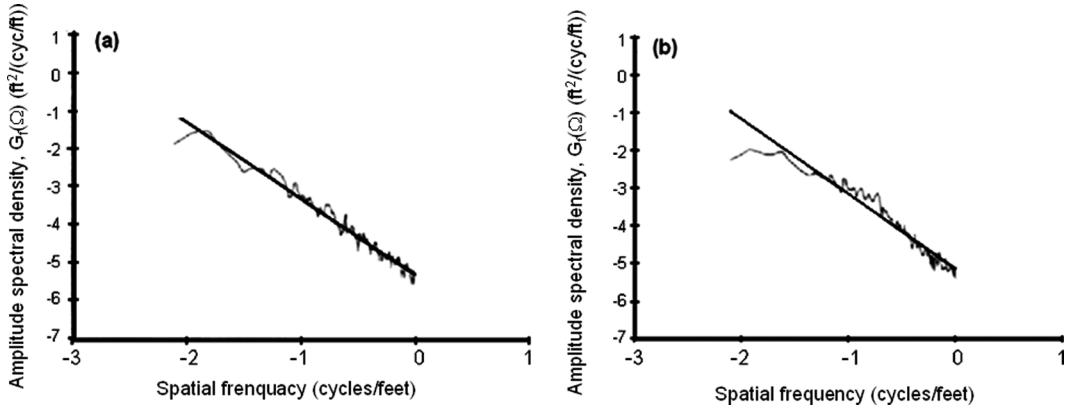

Fig. 7 Roughness from equation (15): (a) $n = -2.02$ and measured in Rochester Road (b) $n = -1.99$ and measured in Broken Road and Rochester Road (reproduced from Hrovat [**15**])

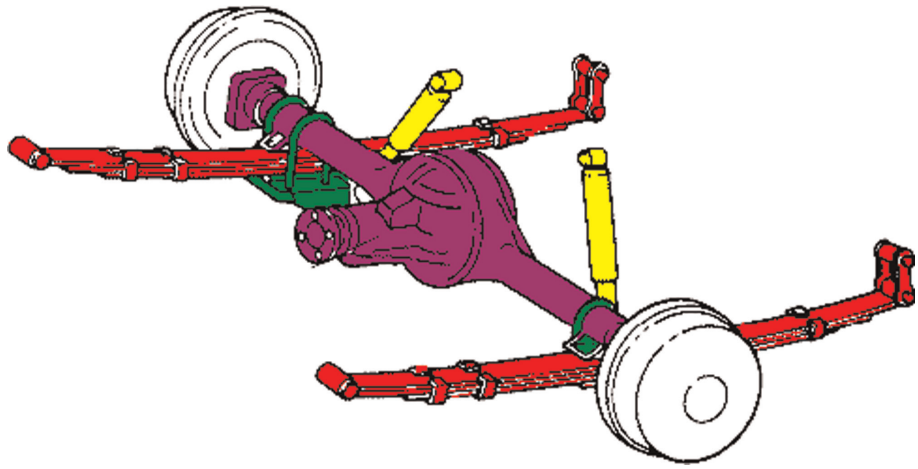

Fig. 8 Leaf spring base Hotchkiss suspension

a drawback, because the designer cannot use physical insight to validate the model.

3.1 Tuning algorithm

The goal here is to develop a system identification process using a constrained non-linear optimization algorithm. The idea is to define a suitable cost function to find the best parameter values to reach the minimum cost. The proposal is to simulate the real vehicle under the same disturbances used in the linear model, and afterwards to compare results through the cost function.

The challenge is to find a simple disturbance that could be easily constructed in experimental tests and that is rich enough to excite the real system so as to allow tuning all the parameters of the model. On the other hand, it is necessary to define a cost function that leads to a stable, robust, and fast solution of the optimum parameter values.

To avoid the use of experimental tests in the development phase, commercial vehicular simulation software is used to generate artificially the tuning data.

The constrained non-linear optimization is used to identify the 13 parameters of the desired low-order model. The optimization is performed using an SQP algorithm available, for example, in MATLAB. The objective is to minimize the 'cost' of the quadratic error between signals produced by the commercial software and signals produced by the simplified model, working under the same disturbances. The function *fminimax* from MATLAB solves the problem

$$\min_{\lambda_{\min}<\lambda<\lambda_{\max}} \{\max[F(\lambda)]\} \tag{16}$$

where $F(\bullet)$ is a MATLAB function created to solve the model equations for the sampled data and which returns a vector with the norms of the differences between the 'measured' and estimated signals.

In equation (16), the vector of parameters is limited by the vectors of minimum and maximum values for each parameter, and the identification problem consists in minimizing the higher values of the cost vector resulting from the function $F(\bullet)$.

The 13 parameters that compose the vector are those presented in Table 1. The limits $\lambda_{\min} < \lambda < \lambda_{\max}$ are established using physical coherence.

The MATLAB function $F(\bullet)$ is an algorithm that performs the following tasks:

(a) calculating the state space matrices using the values of parameters;
(b) transforming the continuous model in a discrete model;
(c) using an iterative approach to calculate the parameters of the difference equation considering the vertical velocities as input signals and producing an output vector with 12 variables, including four body accelerations, four vertical accelerations of the wheels, and four relative displacements in 5 with a sampling rate of 50 *Hz*;
(d) finally calculating the vector of norms of errors between the data produced by the discrete model and the data acquired in experimental tests, as shown in the section 3.1.1.

The optimization process is quite fast, even when run in a notebook, where a time of less than 10 s was necessary for data convergence.

The model identification process is performed using two sets of data, produced using a gutter profile and a hump profile as disturbances. The idea is to reach a model with good performance in several situations of work, called the 'generic' model. Of course, the identification process could be applied to each disturbance case separately, which would naturally lead to better identification for the specific case, but with clear impact for a generic disturbance.

In Appendix 2, the background of SQP and the optimization procedures used in this work are presented. More details about this may be found in references [**30**] and [**31**].

3.1.1 The cost function

The way that the cost vector is calculated from the error norms is an important factor for the convergence and stability of the parameter identification process. The vector of the norms of errors between the data produced by the low-order model and the data acquired in experimental tests (or alternatively from simulations with the commercial software) are calculated as

$$\varepsilon_{2,i} = 50\left\|\hat{\boldsymbol{y}}_{2,i} - \boldsymbol{y}_{2,i}\right\|_2 = 50\sqrt{\sum_{k=1}^{n}\left[\hat{\boldsymbol{y}}_{2,i}(k) - \boldsymbol{y}_{2,i}(k)\right]^2} \tag{17}$$

$$\varepsilon_{3,i} = 2\left\|\hat{\boldsymbol{y}}_{3,i} - \boldsymbol{y}_{3,i}\right\|_2 = 2\sqrt{\sum_{k=1}^{n}\left[\hat{\boldsymbol{y}}_{3,i}(k) - \boldsymbol{y}_{3,i}(k)\right]^2} \tag{18}$$

$$\varepsilon_{4,i} = \left\|\hat{\boldsymbol{y}}_{4,i} - \boldsymbol{y}_{4,i}\right\|_2 = \sqrt{\sum_{k=1}^{n}\left[\hat{\boldsymbol{y}}_{4,i}(k) - \boldsymbol{y}_{4,i}(k)\right]^2} \tag{19}$$

$$\zeta = \begin{bmatrix} \varepsilon_{2,1} & \varepsilon_{2,2} & \varepsilon_{2,3} & \varepsilon_{2,4,} & \varepsilon_{3,1} & \varepsilon_{3,2} \\ \varepsilon_{3,3} & \varepsilon_{3,4,} & \varepsilon_{4,1} & \varepsilon_{4,2} & \varepsilon_{4,3} & \varepsilon_{4,4} \end{bmatrix} \tag{20}$$

In equations (17) to (19), the plant output $\boldsymbol{y}_{2,i}$ is the relative displacement vector, $\boldsymbol{y}_{3,i}$ is the body acceleration vector, and $\boldsymbol{y}_{4,i}$ is the acceleration vector of the wheels, in n samples acquired each 0.02 s. The variables $\hat{\boldsymbol{y}}_{\cdot,i}$ are the respective outputs given by the low-order model. The vector ζ is the cost vector.

The weighting values in equations (17), (18), and (19) (50, 2, and 1 respectively) are used to normalize the values of variables, since $\varepsilon_{2,i}$ has displacement units of metres and $\varepsilon_{3,i}$ and $\varepsilon_{4,i}$ have acceleration units of metres per second squared. The weights are also used to give greater importance to the body acceleration and displacement signals, which have less external influence and therefore are less noisy and more reliable than the signals from the wheels. Moreover, the great nonlinearities of the wheels induce larger errors between the experimental and estimated values from the wheel vertical accelerations.

4 RESULTS

This section presents the results obtained in the complete parameter identification of the low-order model represented by equations (11) to (14), using the methodology presented previously.

First, a rough estimation of each parameter is made by means of simple calculations, geometric measurements, and technical information available about the vehicle and its main components.

The SUV used as basis for the identification procedure is a pickup truck with independent suspension at the front and a rigid axle at the rear. The main dimensions and other features of this vehicle are given in Table 2.

Table 2 Identification results

Engine					
Power (kW)	88 (at 5000 r/min)				
Torque (N m)	198 (at 3000 r/min)				
Compression rate	9.4:1				
Fuel	Gasoline				
Fuel volume (l)	2.5				
Dimensions (m)					
Overall length (m)	4.792				
Width (m)	1.763				
Wheel base (m)	2.831				
Front track (m)	1.486				
Rear track (m)	1.455				
Heights					
Roof to the ground, empty (m)	1.722				
Roof to the ground, loaded (m)	1.641				
Free under the vehicle, empty (m)	0.370				
Free under the vehicle, loaded (m)	0.289				
Centre of gravity from the front axle, empty (m)	1.05				
Centre of gravity from the front axle, loaded (m)	1.57				
Centre of gravity to the ground (estimated), empty (m)	0.6–0.75				
Centre of gravity to the ground (estimated), loaded (m)	0.7–1.0				
Weight, load, and masses					
Gross vehicle weight (kgf)	2314				
Maximum load (kgf)	750				
Mass of the driver (kg)	80				
Mass of the curb (kg)	1484				
Mass of the front wheel (kg)	30				
Mass of the rear axle with the wheel (kg)	150				
Sprung masses					
Total sprung mass, minimum (kg)	1354				
Total sprung mass, maximum (kg)	2184				
Front sprung mass, minimum (kg)	853				
Front sprung mass, maximum (kg)	975				
Rear sprung mass, minimum (kg)	501				
Rear sprung mass, maximum (kg)	1209				
Tyres					
Size	215/75R15				
Pressures					
Front tyre pressure, empty (kPa)	227				
Front tyre pressure, loaded (kPa)	310				
Rear tyre pressure, empty (kPa)	227				
Rear tyre pressure, loaded (kPa)	345				
Mechanical properties of the tyres					
Stiffness, minimum (N/m)	75 000				
Stiffness, maximum (N/m)	317 000				
Stiffness, average (N/m)	126 000				
Damping, minimum (N s/m)	340				
Damping, maximum g (N s/m)	4000				
Damping, average (N s/m)	2170				
Suspension					
Stiffnesses					
Front-spring stiffness, minimum (N/m)	28 000				
Front-spring stiffness, maximum (N/m)	35 000				
Front-spring stiffness, nominal (N/m)	32 700				
Rear-spring stiffness, minimum (N/m)	26 000				
Rear-spring stiffness, maximum (N/m)	30 000				
Rear-spring stiffness, nominal (N/m)	27 000				
Front anti-roll bar stiffness, minimum (N/m)	28 000				
Front anti-roll bar stiffness, maximum (N/m)	35 000				
Front anti-roll bar stiffness, nominal (N/m)	32 700				
Rear anti-roll bar stiffness, minimum (N/m)	NA*				
Rear anti-roll bar stiffness, maximum (N/m)	NA*				
Rear anti-roll bar stiffness, nominal (N/m)	NA*				
Forces on the shock absorbers at the velocities (m/s)	0.13	0.26	0.39	0.52	1.05
Front damping force, traction (N)	770	1480	1760	2100	3000
Front damping force, compression (N)	210	380	500	600	950
Rear damping force, traction (N)	550	1270	1540	1700	2510
Rear damping force, compression (N)	260	440	570	750	1150

*NA, not available.

4.1 Tuning using simulations

The identification starts by choosing a specific CALLAS model, the available commercial software. Good correlation between the simulation results and the experimental data is the merit figure to establish which model is the best.

CALLAS models consider several non-linearities, allowing good representation of real vehicles. Non-linearities may include, for example, curves of force versus displacement for tyres and springs, or curves of force versus velocity for shock absorbers, and the kinematics constraints of this kind of vehicle. Missing data not directly available in the chosen model and listed in Table 2 may be estimated on the basis of typical values also available in the database of the software.

The data generated by the chosen model are produced considering a flat road for a vehicle at constant velocity and with a straight trajectory. Unsprung and sprung body motions are simulated for the vehicle passing two kinds of obstacle, as follows:

(a) at 20 km/h, crossing a gutter 0.080 m deep and 0.90 m wide, where the gutter is positioned diagonally relative to the vehicle, so that the left wheel reaches the obstacle before the right wheel;
(b) at 30 km/h, crossing a hump 0.090 m height and 1.2 m wide, where the hump also is positioned diagonally towards the vehicle.

In all simulations, data are generated at 50 *Hz*, to emulate the constraints found in the experimental tests.

The signals extracted from the software are as follows:

(a) four accelerations signals 'measured' at the points where the chassis is connected to the suspension;
(b) four displacement signals induced by the road profile under each tyre;
(c) four relative displacement signals generated by 'measuring' the distance, between each wheel and the vehicle body for the damper's stroke or the springs deflection;
(d) the run elapsed time.

With the simulation data in hand, a seven-DOF vehicle model (low-order model) is then tuned to reproduce the 'real' vehicle behaviour. The model identification process consists in tuning 13 parameters to minimize the quadratic error cost function using signals generated by the commercial software and signals produced by a simplified model for the same disturbance.

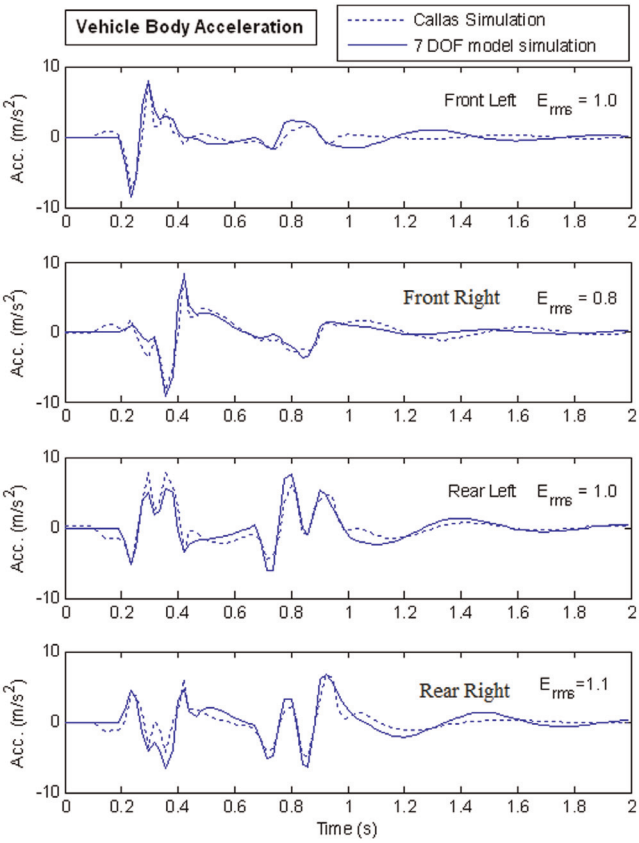

Fig. 9 Simulation of vehicle body acceleration: gutter

To guarantee that the low-order model identification is optimal, this simulation was repeated until the seven-DOF model could be considered reliable and stable (good data repeatability).

To facilitate future control synthesis procedures, the mathematical model obtained by identification is still reduced to the lowest possible order and normalized. Model reduction is achieved by an optimal Hankel norm approximation. In this work, the original fifteenth-order model was successfully reduced to a completely controllable and observable balanced twelfth-order system. More details of order reduction, model balancing, and normalization of the mathematical model may be found in references [**13**] and [**31**].

To illustrate the potential of the identification procedure, sampled results are presented in Figs 9 to 12. Figures 9 and 10 present the simulation results using a model of the commercial software (dashed curves) and the simulation results using the low-order model identified in this work (solid curves) for the vehicle body accelerations in different positions for gutter and hump obstacles respectively. Figures 11 and 12 present the simulation results using CALLAS models (dashed curves) and

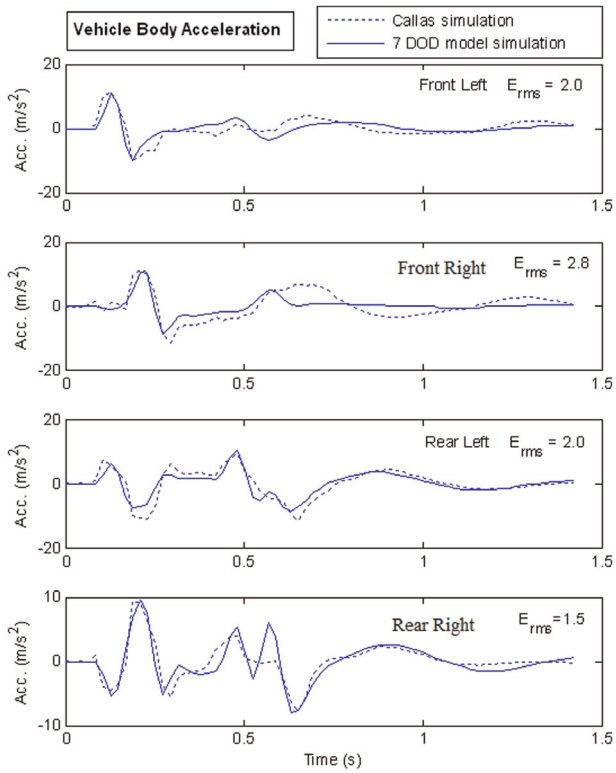

Fig. 10 Simulation of vehicle body acceleration: hump

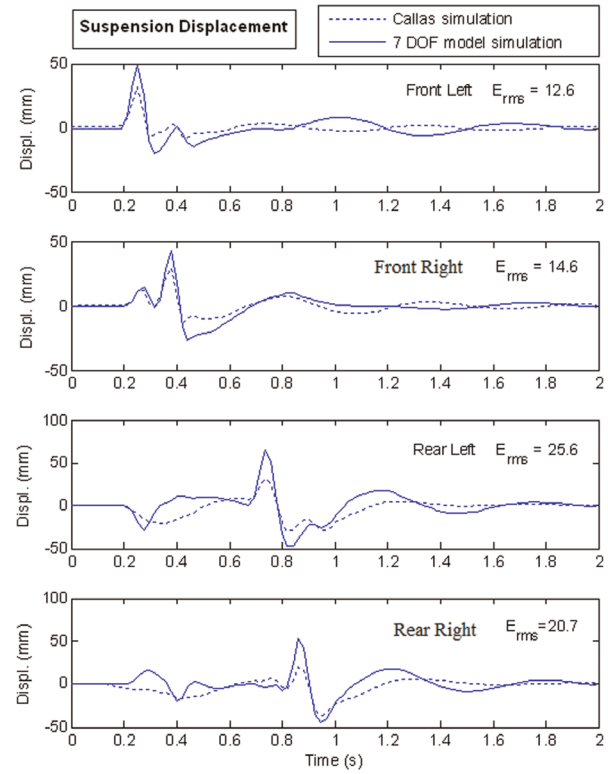

Fig. 11 Simulation of suspension displacements: gutter

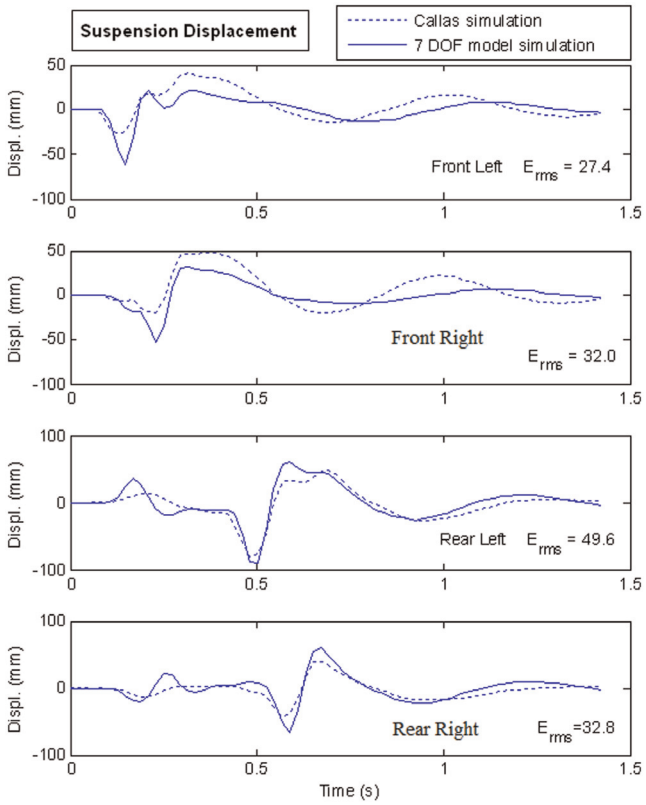

Fig. 12 Simulation of suspension displacements: hump

the simulation results using the low-order model (solid curves) also at the front and rear of the vehicle, for gutter and hump obstacles respectively.

Figures 9 to 12 show that the identified seven-DOF model can effectively reproduce the behaviour of a far more complex CALLAS model. Since there are no significant differences between the results for the two different obstacle simulations (gutter and hump), it is possible to conclude that the identification algorithm is reliable. More on the system identification may be found in reference [**13**].

4.2 Experimental set-up

The next step is to tune the low-order model directly from data measured in a real vehicle. This is achieved in three steps:

(a) construction, calibration, and installation of sensors in the vehicle;
(b) data collection through experiments;
(c) analysis of the experimental data.

Experimental data were acquired using potentiometers to measure the suspension deflections, using accelerometers mounted in the vehicle body over each wheel, and by data acquisition hardware.

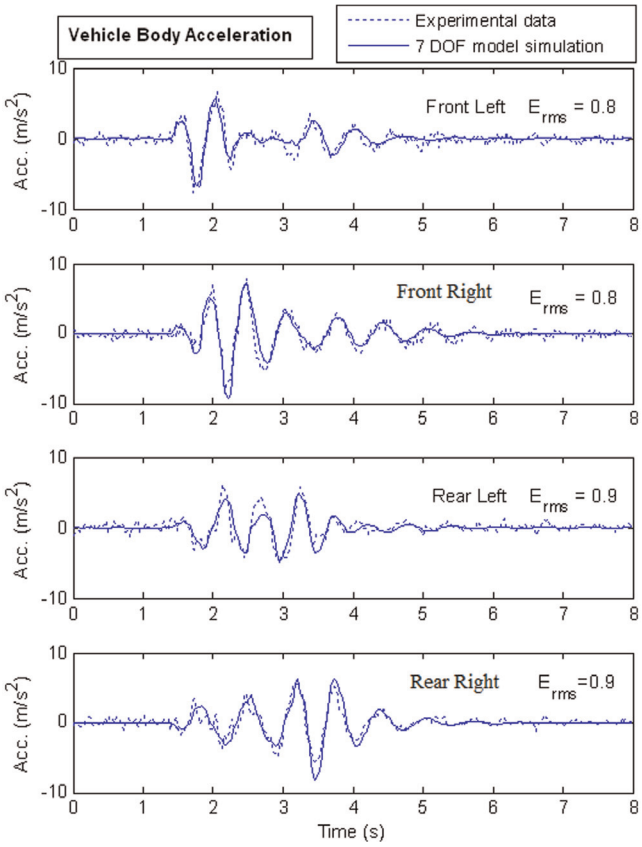

Fig. 13 Experimental body accelerations

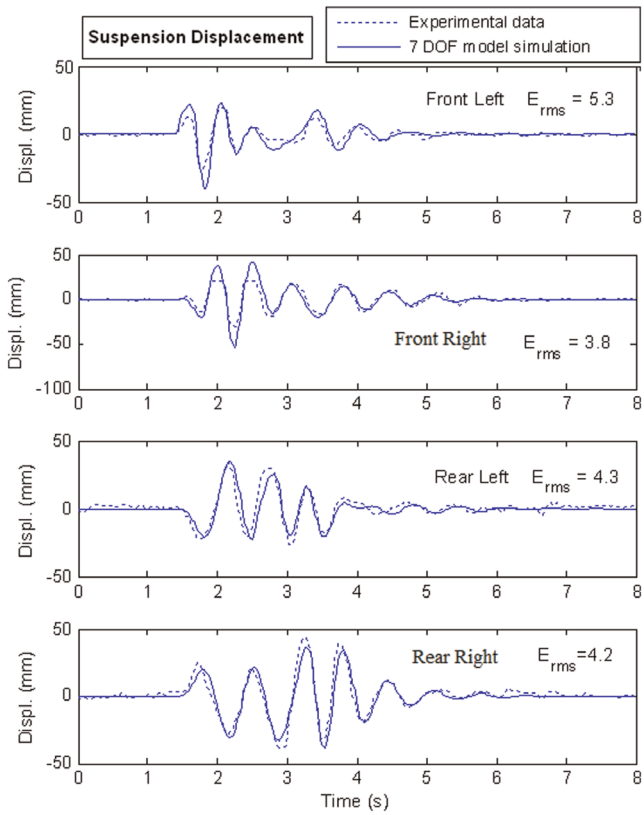

Fig. 14 Experimental suspension displacements

The data acquisition rate is 50 *Hz*, as in the simulation case, and it is imposed by limitations of the available hardware.

The data acquisition uses MATLAB software connected to a target hardware based on a Texas Instruments digital signal processor (TMS320F2812), using the real-time data exchange interface.

The experiment consists of a vehicle which runs at approximately 7 km/h over a flat road and going over a hump similar to that used in the numerical simulations.

The sampled data are used in the identification algorithm. The initial guesses for the parameter values are again those presented in the numerical simulations. The comparison between the seven-DOF model results with experimental data is presented in Figs 13 and 14.

As can be seen, the low-order model (solid curve) represents with satisfactory accuracy the dynamics of the real vehicle during the experimental tests (dashed curve), for both body accelerations and suspension displacements measured for the vehicle front and rear and on both sides. It is important to keep in mind, when evaluating these results, that it is the comparison of a non-linear real mechanical system with a linear low-order model. It is also important to point out that, if the parameters are tuned using another kind of obstacle (a gutter, for example), different parameter values should result. In this case, there are two possibilities: to identify the parameters from all the available experimental data at the same time, producing a generic linear model or, alternatively, to identify the parameters for each set of experimental data, to calculate the mean and variance for each parameter, having a measure of model uncertainties, which is very useful for robust observer and controller design.

5 CONCLUSIONS

The main goal was to develop a methodology for the fast identification of parameters of a low-order model for an SUV suspension using experimental data. This was fully attained.

The use of commercial vehicle simulator software in the early stages of the model identification process led to very satisfactory technical results, a shorter development time, and lower costs in comparison with similar conventional procedures. A main advantage of the procedure at the simulation stage is the possibility of producing as much data as necessary using the simulation package instead of experimental data, until a suitable and reliable low-order model is found. The

identification methods developed are very effective and efficient, with very quick convergence and good repeatability. The low-order model identified by this method is also suitable for control applications using a centralized approach, allowing the inclusion of all the coupling between motions and interaction between variables of the system.

The next step in this research is to use the low-order model identified by the method proposed here to develop a robust controller for the SUV active suspension.

REFERENCES

1 **Rao, M. V. C.** and **Prahlad, V.** A turnable fuzzy logic controller for vehicle-active suspension systems. *Fuzzy Sets Systems*, 1997, **85**, 11–21.

2 **Stutzs, L. T.** and **Rochinha, F. A.** A comparison of control strategies for magnetorheological vehicle suspension systems. In Proceedings of the 11th International Symposium on *Dynamic problems in mechanics* (DINAME XI), Ouro Preto, Minas Gerais, Brazil, 2005.

3 **Hać, A., Youn, I.,** and **Chen, H. H.** Control of suspensions for vehicles with flexible bodies. Part I: active suspensions. Trans ASME, *J. Dynamic Systems, Measmt Control*, 1996, **118**, 508–517.

4 **Ackermann, J.** Robust control prevents car skidding. *IEEE Control Systems Mag.*, 1997, **17**(3), 23–31.

5 **Odenthal, D., Bünte, T.,** and **Ackermann, J.** Nonlinear steering and braking control for vehicle rollover avoidance. In Proceedings of the Fifth European Control Conference (ECC'99), Karlsruhe, Germany, 31 August–3 September 1999.

6 **Tsao, Y. J.** and **Chen, R.** The design of an active suspension force controller using genetic algorithms with maximum stroke constraints. *Proc. IMechE, Part D: J. Automobile Engineering*, 2001, **215**(3), 317–327. DOI:10.1243/0954407011525638.

7 **Simon, D. E.** and **Ahmadian, M.** An alternative semi-active control method for sport utility vehicles. *Proc. IMechE, Part D: J. Automobile Engineering*, 2002, **216**(2), 125–139. DOI: 10.1234/0954407021528977.

8 **da Cruz, J. J., Bittar, A., da Costa, E. A.,** and **Sales, R. M.** Control and optimization of the electromagnetic suspension operation of a MAGLEV vehicle. In Proceedings of the 17th International Congress on *Mechanical engineering* (COBEM 2003), São Paulo, Brazil, 10–14 November 2003, ABCM Symposum Series in Mechatromcs, vol. 1, 2004, 150–158. (Barzilian Society of Mechanical Sciences and Engineering, Rio de Janeiro).

9 **Yamamura, S., Ohnishi, K.,** and **Masada, E.** Theory of control system of electromagnetically levitated bogie truck. *Electl Engng Japan*, 1979, **99**(6), 62–69.

10 **Schittkowski, K.** NLQPL: A FORTRAN-subroutine solving constrained nonlinear programming problems. *Ann. of Op. Res.*, 1985, **5**, 485–500.

11 **Brayton, R. K., Director, S. W., Hachtel, G. D.,** and **Vidigal, L.** A new algorithm for statistical circuit design based on quasi-Newton methods and function splitting. *IEEE Trans Circuits Systems*, 1979, **26**, 784–794.

12 **Thompson, A. G.** An optimal suspension for an automobile on a random road. SAE paper 790478, 1979.

13 **Crivellaro, C.** *Controle robusto de suspensão semiativa para caminhonetes utilizando amortecedores magneto-reológicos.* PhD Thesis, Polytechnic School of University of São Paulo, São Paulo, Brazil, 2008.

14 **Hać, A.** Adaptive control of vehicle suspension. *Veh. System Dynamics*, 1987, **16**, 57–74.

15 **Hrovat, D.** Survey of advanced suspension developments and related optimal control applications. *Automatica*, 1997, **33**(10), 1781–1817.

16 **Gillespie, T. D.** *Fundamentals of vehicle dynamics*, 1994 (SAE International, Warrendale, Pennsylvania).

17 **Sevin, E.** and **Pilkey, W. D.** Optimum shock and vibration isolation. Report, The Shock and Vibration Information Center, US Department of Defense, Washington, DC, USA, 1971.

18 **Smith, R. E.** Amplitude characteristics of Dearborn test track roadways. Technical Memorandum SRM-82–26, Ford Motor Company, Dearborn, Michigan, USA, 1982.

19 **Stone, R.** and **Ball, J. K.** *Automotive engineering fundamentals*, 2004, 612.

20 **Ibrahim, S. R.** and **Mikulcik, E. C.** A method for the direct identification of vibration parameters from the free response. *Shock Vibr. Bulln*, 1977, **47**(4), 183–198.

21 **Vold, H., Kundrat, J., Rocklin, G. T.,** and **Russel, R.** A multi-input modal estimation algorithm for minicomputers. SAE paper 820194, 1982.

22 **Juang, J. N.** and **Pappa, R. S.** An eigensystem realization algorithm for modal parameter identification and model reduction. *J. Guidance, Control Dynamics*, 1985, **8**(5), 620–627.

23 **Zhang, I., Kanda, H., Brown, D. L.,** and **Allemang, R. J.** A polyreference frequency domain method for modal parameter identification. In Proceedings of the 1985 ASME Design Engineering Technical Conference 1985, paper 85-DET-106 (ASME, New York).

24 **Richardson, M. H.** and **Formenti, D. L.** Parameter estimation from frequency response measurements using rational fraction polynomials. In Proceedings of the First International Conference on *Modal analysis*, 1982, pp. 167–180.

25 **Vold, H.** Orthogonal polynomials in the polyreference method. In Proceedings of the 11th International Conference on Modal Analysis, Leuven, Belgium, 1986.

26 **Van der Auweraer, H.** and **Leuridan, J. M.** Multiple input orthogonal polynomial parameter estimation. *Mech. System Signal Processing*, 1987, **1**(3), 259–272.

27 **Shih, C. Y., Tsuci, Y. G., Allemang, R. J.,** and **Brown, D. L.** A frequency domain global parameter estimation method for multiple reference frequency response measurements. *Mech. System Signal Processing*, 1988, **2**(4), 349–365.

28 **Shih, C. Y., Tsuci, Y. G., Allemang, R. J.,** and **Brown, D. L.** A frequency domain global parameter estimation method for multiple reference frequency response measurements. In Proceedings of the 6th International Modal Analysis Conference, Orlando, Florida, 1988, pp. 389–396.

29 **Williams, R., Crowley, J. R.,** and **Vold, H.** The multivariate modal indicator function in modal analysis. In Proceedings of the Third International Conference on Modal Analysis, Orlando, Florida, 28–31 January 1985.

30 **Crivellaro, C.** and **Alves, S.** Phenomenological model of a magneto-rheological damper for semi-active suspension control design and simulation. SAE paper 2006-01-2520, 2006.

31 **Crivellaro, C., Tamai, E. H.,** and **Donha, D. C.** Four-wheel vehicle suspension modeling for control system development. In Proceedings of the 18th International Congress of Mechanical Engineering (COBEM2005), Ouro Preto, Minas Gerais, Brazil, 6–11 November 2005.

32 **Biggs, M. C.** *Constrained minimization using recursive quadratic programming. Toward global optimization* (Eds L. C. W. Dixon and G. P. Szergo), 1975, pp. 341–349 (North-Holland, Amsterdam).

33 **Han, S. P.** A globally convergent method for nonlinear programming. *J. Optimization Theory Applic.*, 1977, **22**(3), 297–309.

34 **Powell, M. J. D.** The convergence of variable metric methods for nonlinearly constrained optimization calculations. In *Nonlinear programming 3* (Eds O. L. Mangasarian, R. R. Meyer, and S. M. Robinson), 1978, pp. 27–63 (Academic Press, London).

35 **Powell, M. J. D.** A fast algorithm for nonlinearly constrained optimization calculations. In *Numerical analysis* (Ed. G. A. Watson), Lecture Notes in Mathematics, **630**, 1978, pp. 144–157 (Springer, New York).

36 **Gill, P. E., Murray, W.,** and **Wright, M. H.** *Practical optimization*, 1981 (Academic Press, London).

37 **Powell, M. J. D.** Variable metric methods for constrained optimization. In *Mathematical programming: the state of the art* (Eds A. Bachem, M. Grotschel, and B. Korte), 1983, pp. 288–311 (Springer Berlin).

38 **Fletcher, R.** *Practical methods of optimization*, 1987 (John Wiley, New York).

APPENDIX 1

Notation

A	road roughness parameter
$\mathbf{A}$	plant matrix
$\mathbf{B}_1$	exogenous input matrix
$\mathbf{B}_2$	control inputs matrix
c_a	residual damping coefficient
c_f	damping coefficients of dampers
c_t	damping coefficients of tyres
CALLAS	couple à la limite d'adhesion au sol
$\mathbf{C}_{01}$	$=\text{diag}(c_t, c_t, c_t, c_t)$
$\mathbf{C}_{12}$	$=\text{diag}(c_a, c_a, c_a, c_a)$
$\mathbf{C}_{12}$	$=\text{diag}(c_f, c_f, c_f, c_f)$
$\mathbf{C}_1$	output matrix of observations $\boldsymbol{y}_1$
$\mathbf{C}_2$	output matrix relative to $\boldsymbol{y}_2$
$\mathbf{C}_3$	output matrix relative to $\boldsymbol{y}_3$
d	semi-axle length
d_r	length of the rear semi-axis
DOF	degree of freedom
$\mathbf{D}_{i\bullet}$	direct input matrix of disturbance in the observations
$\mathbf{D}_{\bullet i}$	direct input matrix of control in the observations
$f(x)$	real scalar objective function
$F(\bullet)$	MATLAB minimax function
$F_i(\boldsymbol{x})$	force values sampled from model simulation
F_i^*	force values sampled of from experimental test
$\boldsymbol{F}_1(t)$	wheel forces
$\boldsymbol{F}_2(t)$	forces from the suspension upon the vehicle sprung body
GAM	goal attainment method
$\mathbf{G}(\boldsymbol{x})$	vector function
$\mathbf{H}$	Hessian of the Lagrangian
$\mathbf{H}_k$	approximation of the Hessian matrix
$\mathrm{I}_{\bullet\times\bullet}$	indentity matrix
J_θ	moment of inertia of the sprung mass around the transverse vehicle axis x
J_φ	moment of inertia of the sprung mass around the transverse vehicle axis y
J_3	moment of inertia of the rear axle
k_t	stiffness coefficient of the tyres
k_{tb}	stiffness coefficient of the torsion bar
$\mathbf{K}_{01}$	$=\text{diag}(c_k, c_k, c_k, c_k)$
l_1	distance from the centre of gravity to the front axle
l_2	distance from the centre of gravity to the rear axle
LQG	linear quadratic gaussian
$L(x, \lambda)$	Lagrangian function
$\mathbf{L}_1$	transformation matrix relating $\dot{\boldsymbol{z}}_1(t)$ to the vertical velocities of the four wheels
$\mathbf{L}_2$	transformation matrix relating the vertical displacements of the sprung vehicle body at the suspension connection points to heave

m_1	front-wheel mass
m_2	sprung mass of the vehicle
m_3	rear-wheel mass
MIMO	multiple input multiple-output
$\mathbf{M}_1$	$=\text{diag}(m_1, m_1, m_3, J_3)$
$\mathbf{M}_2$	$=\text{diag}(m_2, J_\phi, J_\theta)$
n	integer constant
NA	not available
PSD	power spectral density
QP	quadratic programming
SERA-CD	Société d'Études et Réalisations Automobiles
SQP	sequential quadratic programming
SUV	sport utility vehicle
$\boldsymbol{u}(t)$	control vector
$\boldsymbol{w}(t)$	input disturbances
$\boldsymbol{x}$	vector of variables
$\boldsymbol{x}(t)$	state vector $=\left[\boldsymbol{z}_{01}(t) \quad \boldsymbol{z}_{12}(t) \quad \dot{\boldsymbol{z}}_1(t) \quad \dot{\boldsymbol{\xi}}(t)\right]^T$
$\boldsymbol{y}_1(t)$	outputs of the relative displacements $=\boldsymbol{z}_{01}(t)$
$\boldsymbol{y}_2(t)$	output of sprung mass acceleration over each wheel
$\boldsymbol{y}_{2,i}$	relative displacement vector from experiment or from commercial software
$\boldsymbol{y}_3(t)$	outputs of the relative displacements between the centre of each wheel and the point of connection in the vehicle body $=\boldsymbol{z}_{12}(t)$
$\boldsymbol{y}_{3,i}$	body acceleration vector from experiment or from commercial software
$\boldsymbol{y}_{4,i}$	acceleration vector of the wheels from experiment or from commercial software,
$\hat{\boldsymbol{y}}_{2,i}$	relative displacement vector from the low-order model
$\hat{\boldsymbol{y}}_{3,i}$	body acceleration vector from the low-order model
$\hat{\boldsymbol{y}}_{4,i}$	acceleration vector of the wheels from the low-order model
$\boldsymbol{z}_{\text{CG}}(t)$	heave motion of the centre of gravity
$\boldsymbol{z}_{01}(t)$	vector of the relative displacements between the ground and each wheel
$\boldsymbol{z}_{12}(t)$	vector of relative displacements between the centre of each wheel and the point of connection in the vehicle body
$\dot{\boldsymbol{z}}_0(t)$	vertical velocities applied by the ground in each wheel
$\dot{\boldsymbol{z}}_{01}(t)$	relative velocities between the ground and each wheel
$\dot{\boldsymbol{z}}_1(t)$	vertical velocities of the front wheels, the vertical velocity of the rear axis, and its angular velocity
$\dot{\boldsymbol{z}}_{12}(t)$	relative velocities between the centre of each wheel and the point of connection in the vehicle body
α_k	step length
γ	objective function
$\varepsilon_{2,i}$	vector norm of relative displacement errors
$\varepsilon_{3,i}$	vector norm of body acceleration errors
$\varepsilon_{4,i}$	vector norm of wheel acceleration errors
ζ	cost vector
$\theta(t)$	roll angle of the vehicle body
λ	Lagrange multiplier
$\lambda_{\max}$	superior limit of λ
$\lambda_{\min}$	inferior limit of λ
$\varphi(t)$	pitch angle of the vehicle body
$\boldsymbol{\xi}(t)$	$=\left[z_{\text{CG}}(t) \quad \varphi(t) \quad \theta(t)\right]^{\text{T}}$
$\Psi(\boldsymbol{x}, \gamma)$	merit function
ω_i	weighting factor
Ω	spatial frequency (or the wave number)
$\boldsymbol{0}_{\bullet\times\bullet}$	null matrix

APPENDIX 2

SQP background

SQP methods represent the state of the art in nonlinear programming methods. Schittkowski [**10**], for example, implemented and tested a version that outperforms every other tested method in terms of efficiency, accuracy, and percentage of successful solutions, over a large number of test problems. The method allows Newton's method for constrained optimization to be closely mimicked, just as for unconstrained optimization [**32–35**]. Overviews on SQP can be found in references [**10**] and [**36**] to [**38**].

A general problem is stated as

$$\min_x [f(\boldsymbol{x})]$$

subject to

$$\begin{aligned} &G_i(\boldsymbol{x}) = 0 \ (i=1, 2, \ldots, m_{\text{e}}) \\ &G_i(\boldsymbol{x}) \leqslant 0 \ (i=m_e+1, \ldots, m) \end{aligned} \tag{21}$$

where $f(\boldsymbol{x})$ is a real scalar objective function, $\boldsymbol{x}$ is the vector of length n design parameters, $\boldsymbol{G}(\boldsymbol{x})$ is a vector function of length m with the equality and inequality constraints evaluated at $\boldsymbol{x}$.

Given the description of the general problem (equation (21)), a quadratic programming (QP) subproblem is formulated on the basis of a quadratic approximation of the Lagrangian function

$$L(\boldsymbol{x},\lambda)=f(\boldsymbol{x})+\sum_{i=1}^{m}\lambda_i n g_i(\boldsymbol{x}) \tag{22}$$

The QP subproblem is formally posed as

$$\begin{aligned} &min\left(\tfrac{1}{2}\boldsymbol{d}^{\mathrm{T}}\mathbf{H}_k\boldsymbol{d}\right)+\nabla f(\boldsymbol{x}_k)^{\mathrm{T}}\boldsymbol{d}\\ &\nabla g_i(\boldsymbol{x}_k)^{\mathrm{T}}d+g_i(\boldsymbol{x}_k)=0, i=1,2,,m_{\mathrm{e}}\\ &\nabla g_i(\boldsymbol{x}_k)^{\mathrm{T}}d+g_i(\boldsymbol{x}_k)<0, i=m_{\mathrm{e}}+1,\ \ldots,\ m \end{aligned} \tag{23}$$

The solution is used to form the next step as

$$\boldsymbol{x}_{k+1}=\boldsymbol{x}_k+\alpha_k d_k \tag{24}$$

where the parameter α_k is the step length determined by an appropriate line search procedure that guarantees a sufficient decrease in the merit function. The matrix $\mathbf{H}_k$ is a positive definite approximation of the Hessian matrix of the Lagrangian function, given by equation (22). $\mathbf{H}_k$ can be updated by any of the quasi-Newton methods.

The GAM has the advantage of being posed as a non-linear programming problem so that characteristics of the problem can be exploited in the programming algorithm. In SQP, the choice of a merit function for a line search is not easy because, in many cases, it is difficult to establish the relative importance between improvements in the objective function and the reduction in the constraint violations. To overcome this problem, a number of different schemes for constructing the merit function are now available (see, for example, reference [**10**]). In the GAM, an appropriate merit function may be achieved by posing the problem as a minimax problem according to

$$\min_{\boldsymbol{x}\in\Re^n}\left(\max_i \Lambda_i\right) \tag{25}$$

where

$$\Lambda_i=\frac{F_i(\boldsymbol{x})-F_i^*}{\omega_i},\quad i=1,\ldots,m \tag{26}$$

Following the arguments of Brayton *et al.* [**11**] for the minimax optimization using SQP, the GAM of equation (25) is formalized as

$$\Psi(\boldsymbol{x},\gamma)=\gamma+\sum_{i=1}^{m} r_i \max_{i=1}^{m}\left[0,F_i(\boldsymbol{x})-\omega_i\gamma-F_i^*\right] \tag{27}$$

When the merit function expressed in equation (25) is used as the basis of a line search procedure, then, although $\Psi(\boldsymbol{x},\ \gamma)$ might decrease for a step in a given search direction, the function $\max(\Lambda_i)$ might paradoxically increase. This is similar to accepting a degradation in the worst-case objective. Since the worst-case objective accounts for the value of the objective function γ, this is equivalent to accepting a step that ultimately increases the objective function to be minimized. Conversely, the merit function $\Psi(\boldsymbol{x},\ \gamma)$ might increase when the function $\max(\Lambda_i)$ decreases, which would imply the rejection of a step that improves the worst-case objective.

Following the idea of Brayton *et al.* [**11**], a solution is to set $\Psi(\boldsymbol{x})$ equal to the worst-case objective, according to

$$\Psi(\boldsymbol{x})=\max_i(\Lambda_i) \tag{28}$$

A common problem in the GAM is to use a weighting coefficient equal to zero to incorporate hard constraints. The merit function given by equation (28) then becomes infinite for arbitrary violations of the constraints. To overcome this problem while still retaining the features of equation (28), a modified merit function is

$$\Psi(\boldsymbol{x})=\sum_{i=1}^{m}\left\{\begin{array}{ll} r_i\ \max\left[0,F_i(\boldsymbol{x})-\omega_i\gamma-F_i^*\right] & \text{if } \omega_i=0\\ \max_i(\Lambda_i) & \text{otherwise}\end{array}\right\} \tag{29}$$

Another feature that can be exploited in SQP is the objective function itself. From the Kharash–Kuhn–Tucker equations, it can be shown that the approximation to the Hessian **H** of the Lagrangian should have zeros in the rows and columns associated with the variable γ. However, this property does not appear if **H** is initialized as the identity matrix. **H** is therefore initialized and always forced to have zeros in the rows and columns associated with γ.

These changes make the Hessian, **H**, indefinite. Therefore, **H** is set to have zeros in the rows and columns associated with γ, except for the diagonal element, which is set to a small positive number (e.g. 10^{-10}). This allows the use of the fast converging positive definite QP method, described as a QP subproblem.

The GAM is based on a minimax problem. In the optimization problem posed in equations (25) and (26), F_i^* is a force, the data for which were obtained

in experimental results and we composed of 3000 samples. $F_i(\boldsymbol{x})$ in equation (26) corresponds to the 3000 force values sampled from the model simulation results, which were calculated iteratively by numerically solving the model differential equations (1) and (2) at each step of the optimization process, employing a Runge–Kutta 45 algorithm. The simulations were performed using the displacements obtained in the experiments and the calculated velocity of the piston rod for determination of the force generated in the damper model.

The model-fitting problem corresponds to finding the vector x which better fits the model behaviour given by the experimental data. To avoid local minima points, initial values were defined for these parameters so that the behaviour of the model could perform very similarly to experimental results. This was achieved through a careful physical analysis of each parameter and by a suitable choice. Also upper and lower bound limits were defined for the parameter values, to restrict the problem to a narrow space of possible parameters.

To verify the model robustness, the parameter identification process was applied only to the experiment with amplitude displacements in the range ± 15 mm. The identified model was then tested with the second experimental data set, where amplitude displacements of piston rod were in the ± 30 mm range.

The results of parameter identification process using the optimization algorithm are shown in Table 2 (see section 4.2).